An Observational Study of the Final Breakdown of the Southern Hemisphere Stratospheric Vortex in 2002

YVAN J. ORSOLINI

Norwegian Institute for Air Research, Kjeller, Norway

CORA E. RANDALL

Laboratory for Atmospheric and Space Physics, University of Colorado, Boulder, Colorado

GLORIA L. MANNEY

Jet Propulsion Laboratory, California Institute of Technology, Pasadena, California, and Department of Natural Sciences, New Mexico Highlands University, Las Vegas, New Mexico

DOUGLAS R. ALLEN

U.S. Naval Research Laboratory, Washington, D.C.

(Manuscript received 22 May 2003, in final form 1 March 2004)

ABSTRACT

The 2002 Southern Hemisphere final warming occurred early, following an unusually active winter and the first recorded major warming in the Antarctic. The breakdown of the stratospheric polar vortex in October and November 2002 is examined using new satellite observations from the Michelson Interferometer for Passive Atmospheric Sounding (MIPAS) instrument aboard the European Space Agency (ESA) *Environment Satellite* (*ENVISAT*) and meteorological analyses, both high-resolution fields from the European Centre for Medium-Range Weather Forecasts and the coarser Met Office analyses. The results derived from MIPAS observations are compared to measurements and inferences from well-validated solar occultation satellite instruments [Halogen Occultation Experiment (HALOE), Polar Ozone and Aerosol Measurement III (POAM III), and Stratospheric Aerosol and Gas Experiments II and III (SAGE II and III)] and to finescale tracer fields reconstructed by transporting trace gases based on MIPAS or climatological data using a reverse-trajectory method. These comparisons confirm the features in the MIPAS data and the interpretation of the evolution of the flow during the vortex decay revealed by those features. Mapped ozone and water vapor from MIPAS and the analyzed isentropic potential vorticity vividly display the vortex breakdown, which occurred earlier than usual. A large tongue of vortex air was pulled out westward and coiled up in an anticyclone, while the vortex core remnant shrank and drifted eastward and equatorward over the South Atlantic. By roughly mid-November, the vortex remnant at 10 mb had shrunk below scales resolved by the satellite observations, while a vortex core remained in the lower stratosphere.

1. Introduction

The meteorology of the Southern Hemisphere (SH) stratosphere was highly unusual in the winter and spring of 2002. The first major stratospheric sudden warming ever observed in the SH occurred in late September, characterized by an episodic reversal of zonal-mean zonal winds from westerlies to easterlies over the high southern latitudes. The strong amplification of planetary waves propagating up from the lower stratosphere led to a splitting of the polar vortex into two lobes (e.g., Allen et al. 2003; Newman and Nash 2005). These events were accompanied by splitting of the Antarctic ozone hole (Hoppel et al. 2003; Eskes et al. 2005). The meteorological situation had in fact been very disturbed throughout the winter, with several precursory pulses of increased planetary wave amplitude and fluxes from May to August (Allen et al. 2003). While large-amplitude planetary waves and fluxes usually maximize in the SH spring (Yamazaki and Mechoso 1985; Mechoso et al. 1988; Hirota et al. 1990; Manney et al. 1991), their magnitudes were exceptionally large in September 2002. By mid-October, a weakened polar

Corresponding author address: Dr. Yvan J. Orsolini, Norwegian Institute for Air Research, Instituttveien 18, N-2027 Kjeller, Norway.
E-mail: orsolini@nilu.no

vortex recovered a pole-centered position, as one of the two lobes was expelled to the middle latitudes, where it rapidly mixed with extravortex air. Wave heat fluxes from the lower stratosphere intensified anew in the second half of October and were rapidly followed by the final warming, which occurred earlier than in previous years (Allen et al. 2003).

The final warming of the SH polar stratosphere and the disappearance of the cyclonic polar vortex normally occur in November or early December. The warming characteristically shows downward progression with time, and the vortex is longer-lived in the lower stratosphere (Manney et al. 1994a,b; Waugh and Randel 1999, hereafter WR99). Climatological diagnostics of the vortex breakdown involves definitions of a threshold size or wind speed, below which the vortex ceases to exist as an entity. Exact breakdown dates are sensitive to the parameter choice, albeit weakly so (Waugh et al. 1999). Area diagnostics are commonly used in stratospheric meteorology (Butchart and Remsberg 1986; Manney et al. 1994a). The area within isentropic potential vorticity (PV) contours can be converted into an equivalent latitude, and the location of the strong PV latitudinal gradient identifies the vortex edge. The equivalent latitude of a PV contour is the latitude bounding a polar cap of the same area as the one enclosed by the PV contour. At 850 K (475 K), the vortex edge is normally located at an equivalent latitude near 60°S in late winter and, by the end of October, retreats poleward to a mean equivalent latitude of 75°S (70°S)+/−5° depending on the given year (WR99).

Processes leading to the vortex breakdown in the SH springs of 1982 and 1992 have been documented by Farrara and Mechoso (1986) and Lahoz et al. (1996), respectively. The latter study used global analyses from the Met Office (UKMO) and satellite observations of water vapor from the Microwave Limb Sounder (MLS) instrument aboard the *Upper Atmosphere Research Satellite*. Both studies showed that wintertime anticyclones develop over preferred geographical regions. The latter also showed that springtime eastward-traveling anticyclones slow down as they approach the 90°E–180° sector and ultimately coalesce in a large, persistent stationary anticyclone, located south of Australia. Using 9 yr of Southern Hemisphere springtime meteorological data, Harvey et al. (2002) show that these "Australian high" anticyclones are climatological features that each year repeatedly form at longitudes between about 180° and 270°E and then migrate westward into the 90°E–180° sector where they remain quasi-stationary. Harvey et al. (2002) further show that these anticyclones gradually move over the pole during the final warming. While the winter vortex is preferably found at western longitudes (especially the 0°–90°W quadrant), it progresses eastward in the final warming stage (WR99).

We examine the vortex breakdown in October and November 2002, using two new datasets. First, we use operational meteorological analyses produced by variational data assimilation at the European Centre for Medium-Range Weather Forecasts (ECMWF). These are now available at unprecedented resolution and exhibit exquisite detailed fluid dynamical–like features, such as thin filaments or small vortices (Simmons et al. 2005). Second, we use satellite observations of ozone and water vapor from the Michelson Interferometer for Passive Atmospheric Sounding (MIPAS) instrument aboard the *Environment Satellite* (*ENVISAT*) launched in March 2002. We will demonstrate that these new satellite observations of minor constituents provide a view of the initial stage of the vortex breakdown as large, coherent remnants form and begin to mix down. In section 2, we briefly describe the MIPAS instrument, and in section 3, we discuss the meteorological data. The meteorological conditions associated with the breakdown of the vortex are described in section 4, and how these events unfold in the ozone and water vapor distributions measured by MIPAS are discussed in section 5. The next two sections compare mapped MIPAS water vapor to a passively advected water vapor (section 6) and to validated measurements and inferences from solar occultation instruments (section 7). Conclusions are presented in section 8.

2. MIPAS observations of ozone and water vapor

MIPAS is a limb-scanning infrared interferometer that measures temperature, ozone, water vapor, and a whole suite of other minor atmospheric constituents. Additional instrument characteristics are described in Glatthor et al. (2005). The *ENVISAT* sun-synchronous polar orbit provides global coverage with nearly 14 orbits per day. The along-track sampling corresponds to a horizontal resolution of approximately 500 km. Observations range from the tropopause to the mesosphere and have a vertical resolution of 3–4 km.

Operational retrievals are performed by the European Space Agency (ESA), and the first date available to us through a validation and calibration program was 24 October 2002. We have used 1 month of observations of ozone and water vapor, starting on that date, from the ESA MIPAS fast-delivery "Meteo-Products." Along-track ozone and water vapor mixing ratios were interpolated onto potential temperature levels calculated from retrieved temperature profiles.

Ozone and water vapor maps have been produced by binning along-track data in longitude (36° bins) and latitude (10° bins). The data have been lumped in 3-day periods prior to spatial binning, in order to achieve global coverage in the presence of missing orbits in the operational *ENVISAT* dataset. Available data are listed in the Table 1. Missing data have precluded the use of truly synoptic mapping, a technique that has been used to study vortex dynamics and planetary waves in trace species observations from polar-orbiting satellites (Manney et al. 1998). Its use is not so critical

TABLE 1. Number of MIPAS along-track observations at 850 K in the SH used in this study. Data have been recovered from the operational near–real time products from ESA and contain missing data or orbital segments varying from day to day. Note the few observations on 1–3 Nov, a fact that might affect the quality of the maps covering this 3-day period.

Date	No. of obs
24 Oct 2002	179
25 Oct 2002	286
26 Oct 2002	205
27 Oct 2002	60
28 Oct 2002	295
29 Oct 2002	230
30 Oct 2002	259
31 Oct 2002	297
1 Nov 2002	7
2 Nov 2002	1
3 Nov 2002	75
4 Nov 2002	219
5 Nov 2002	206
6 Nov 2002	259
7 Nov 2002	283
8 Nov 2002	196
9 Nov 2002	0
10 Nov 2002	271
11 Nov 2002	276
12 Nov 2002	295
13 Nov 2002	289
14 Nov 2002	254
15 Nov 2002	216
16 Nov 2002	216
17 Nov 2002	190

for slowly moving features such as those studied here. Our maps, while coarse in space and time, capture interesting features of the vortex dynamical evolution in the spring of 2002. A detailed validation of the MIPAS observations is out of the scope of the present study, but we use inferences from solar-occultation measurements and idealized tracer advection to confirm the evolution of the vortex and its remnants as diagnosed in the MIPAS observations.

3. Meteorological data

We use two sets of meteorological analyses in this study. First, we use the very high resolution analyses from the ECMWF to describe in detail the final breakdown of the polar vortex and the ensuing fate of its remnants. The 6-hourly analyses of geopotential height and PV are produced by four-dimensional variational data assimilation and have a maximum resolution of about 0.2° (spectral truncation T511). Equivalent latitudes were calculated with the full T511 resolution. Note that PV is negative in the SH.

The proxy tracer reconstructions on the other hand (section 7) are based on establishing correlations between sparse satellite occultation measurements and PV. Hence, we have relied on the coarser analyses from the Met Office stratosphere–troposphere assimilation system (Swinbank and O'Neill 1994). These data are available once daily at 1200 UTC on a 2.5° latitude by 3.75° longitude grid. While we recognize that the use of a single assimilated dataset might have been more consistent, for the sake of comparing coarse-grained features that are likely to be similar in both sets, we utilize the Met Office data as in Randall et al. (2005) for the proxy tracer reconstructions. Similarly, reverse-trajectory (RT) calculations (section 6) are based on the Met Office analyses as in Manney et al. (2000).

4. The collapse of the SH vortex in early November

During the austral spring 2002, the zonal-mean zonal winds reversed to easterlies in late October at 10 mb (Allen et al. 2003; Krüger et al. 2005). Examination of 42 yr of ECMWF Re-Analysis (ERA-40) covering the years 1960 to 2001 indicates that easterlies do not usually prevail in the November mean at that altitude, as was the case in 2002. Furthermore, only in 1988 and 2002 was the zonal-mean zonal wind at 10 mb westward and exceeded -10 m s^{-1}. The final warming in 2002 hence occurred earlier than usual.

A sequence of PV maps at 850 K (Fig. 1) and geopotential height maps at 10 mb (Fig. 2) shows that the dramatic evolution of the vortex final breakdown in early November is largely governed by vortex interactions:

- On 2 November, a still-closed intact vortex, albeit small, is displaced off the pole, and a tongue of subtropical air is drawn close to the South Pole, crossing over South America and coiling cyclonically around the vortex. We will refer to this tongue as tongue "S."
- By 5 November, the vortex is very elongated, and a large tongue of vortex air is pulled westward and coiled around an anticyclone. We will refer to this tongue as tongue "V."
- By 8 November, this pulling apart of the vortex has intensified, as the anticyclone between Australia and Antarctica drifts further westward, and the collapsing vortex drifts castward over the southern Atlantic. The coiling of tongue V around the anticyclone continues.
- On 11 November, two major pools of vortex air persist over the Western Hemisphere, including tongue V and the vortex core remnant over the southern Atlantic.

The final collapse of the weak vortex in early November as revealed by the detailed PV fields is quite rapid and spectacular. There are ubiquitous small-scale vortices and filaments in the analyzed PV, which remain coherent over several days (Simmons et al. 2005). Intriguingly, the thinning tongue V pulled westward out of the vortex rolls up into a small, coherent cyclonic vortex during 8–11 November (near 40°S and 150°E on 11 November). Both the small eddy and the two

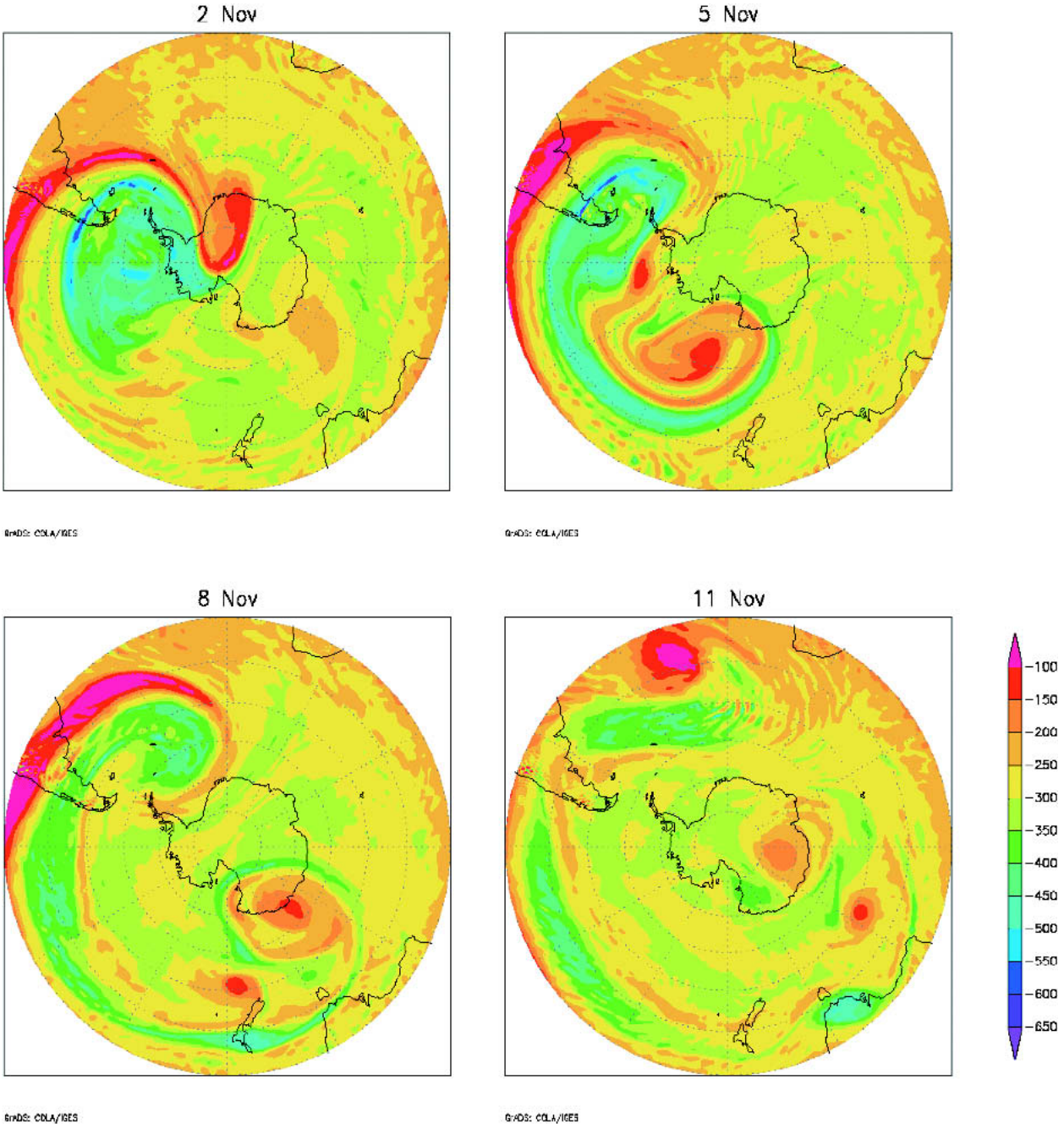

FIG. 1. Stereographic projections of PV at 850 K and 10 mb on 2, 5, 8, and 11 Nov 2002, derived from ECMWF analyses. Depicted latitudes range from the pole to 30°S; 0° longitude is at the top, with east longitudes increasing clockwise. Units are in PV units (PVU, 1 PVU = 10^6 K m^2 kg^{-1} s^{-1}).

branches spiraling outward are clearly visible for several days.

Figure 3a shows PV versus equivalent latitude at 850 K averaged over the periods 24–30 October and 7–13 November. A weak vortex is still present in late October, as shown by the steepened PV gradient starting at 70°S, but what is left of the vortex by mid-November covers a very small area. This would place the breakdown date at 850 K in the first week of November, in conformity with what is shown in the sequence of maps in Figs. 1 and 2.

The vortex breakdown is normally a top-down process, that is, the wind reversal occurs earlier at higher altitudes. That the relationship between PV and equivalent latitude changes little from late October to mid-November (Fig. 4a) at 475 K demonstrates that the

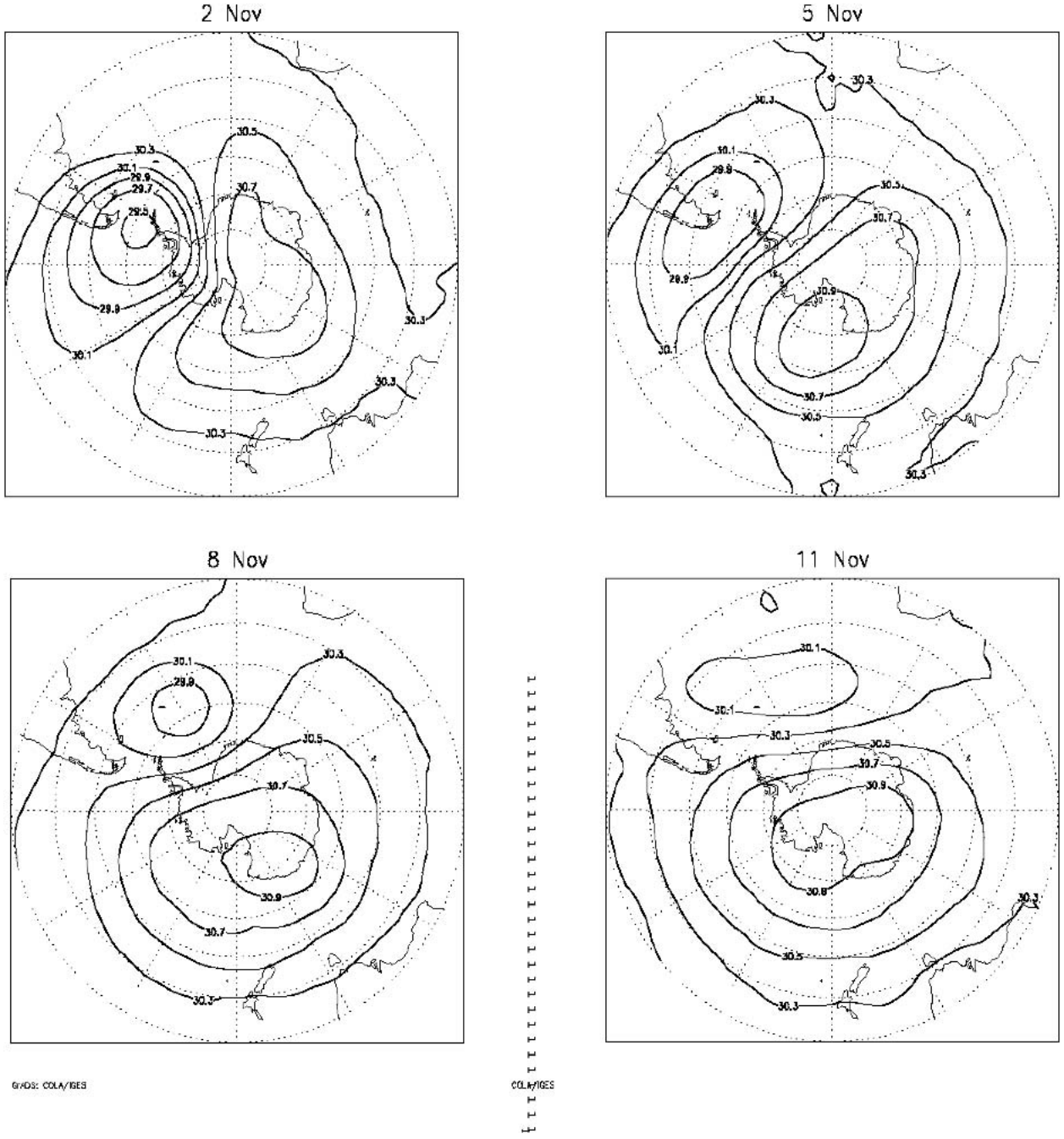

FIG. 2. Same as in Fig. 1, but for geopotential height at 10 mb. Units are in km.

vortex is longer lived at that level than at 850 K. In fact, the vortex area has reduced only slightly by 14–20 November. In Fig. 5, a PV map at 475 K shows the remaining polar vortex breaking in two pieces on 16 November. This longer persistence at lower levels is also consistent with effective diffusivity calculations for this period by Allen et al. (2003) and with the location of the vortex edge at various altitudes described by Konopka et al. (2005).

5. The collapse of the SH vortex in ozone and water vapor observations

Hemispheric maps of minor constituents measured from various satellite instruments have been used in the past to study the dynamics of the polar vortex and associated transport processes (Leovy et al. 1985; Hess 1991; Manney et al. 1993; Lahoz et al. 1996; Manney et al. 1995, 1998). Our investigation of ozone and water

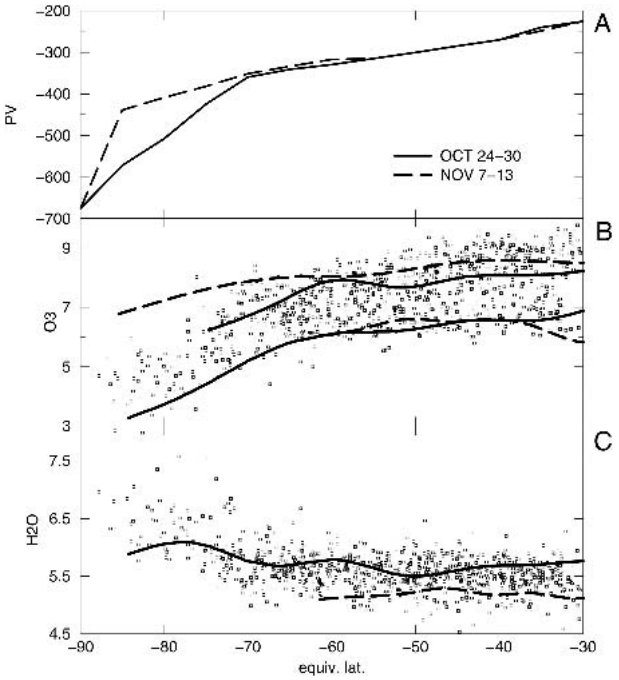

FIG. 3. (a) The PV at 850 K averaged over the periods 24–30 Oct and 7–13 Nov as a function of equivalent latitude. Also shown are (b) ozone and (c) water vapor at 850 K for 24–30 Oct. The data points in (b) and (c) are individual measurements taken from all the along-track MIPAS data collected in the time period over the SH. Ozone and water vapor (ppmv). Relationships between equivalent latitude and ozone for 24–30 Oct, derived from POAM (lower solid curve) and SAGE III (upper solid curve), and for 7–13 Nov, derived from POAM and HALOE (lower dashed curve) and from SAGE II and III (upper dashed curve), are shown in (b). Relationships between water vapor and equivalent latitude determined from POAM for 24–30 Oct (solid curve) and from POAM and HALOE for 7–13 Nov (dashed curve) are shown in (c).

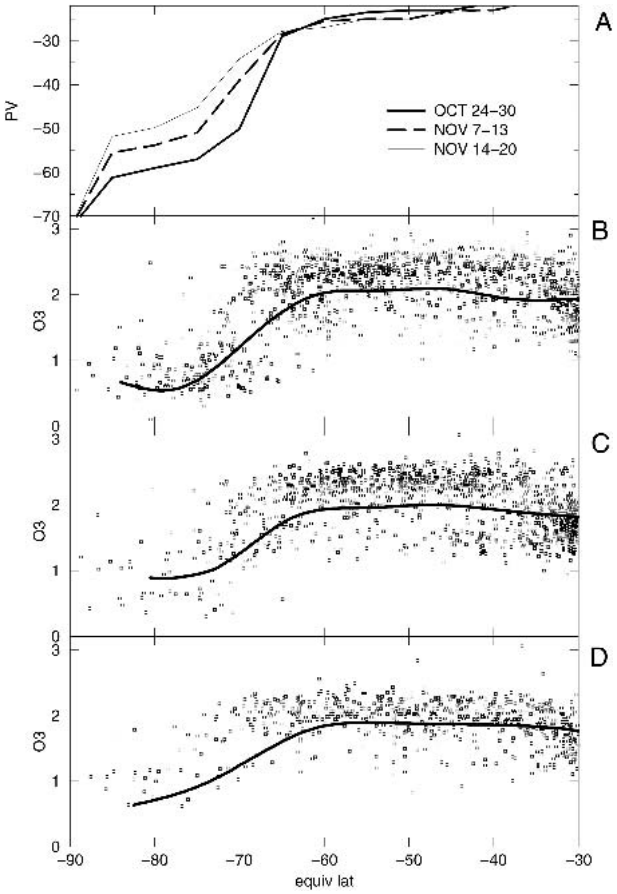

FIG. 4. (a) The PV at 475 K averaged over the periods 24–30 Oct, 7–13 Nov, and 14–20 Nov as a function of equivalent latitude. Also shown are MIPAS ozone for these three periods [(b)–(d)]. These data points are individual measurements taken from all the along-track MIPAS data collected in the time period over the SH. Thick solid curves in (b)–(d) show the relationships between ozone and equivalent latitudes determined from solar occultation data at 475 K for time periods corresponding to the MIPAS data.

vapor transport focuses on altitudes near 30 km, above the layer where chlorine-based catalytic destruction of ozone is activated by heterogeneous chemical processes. Photochemical processes strongly contribute to ozone destruction at those altitudes during the transition to summer as sunlight becomes more abundant. Water vapor, on the other hand, can be treated as a passive tracer over a time scale of several weeks.

Near 30 km, vortex air is depleted in ozone and enriched in water vapor relative to extravortex air. This results partly from diabatic descent of air from the upper regions of the middle atmosphere and partly from the prolonged separation of low- and high-latitude air during the winter (e.g., Manney et al. 1995; Lahoz et al. 1996). The characteristics of vortex air are large (negative) PV, low ozone, and high water vapor mixing ratios. Air masses with these three characteristics are observed by MIPAS in late October at 850 K; in Figs. 3b–c, all along-track MIPAS observations of ozone and water vapor in the SH have been plotted as a function of equivalent latitude for 24–30 October, as was done for PV (Fig. 3a). At equivalent latitudes poleward of 70°S, there is a distinct tendency for sampled air masses to be poorer in ozone and relatively moister than at lower equivalent latitudes. No such characteristic relationship between the tracers and equivalent latitude was found in the 7–13 November period (not shown for brevity). At 475 K, however, ozone-poor air is still observed at equivalent latitudes poleward of 70°S well into November (Figs. 4b–d), in accordance with the PV distribution.

Equivalent latitude and potential temperature cross sections of water vapor throughout the period of interest are shown in Fig. 6, mapped as described by Manney et al. (1999). Water vapor profiles have been combined into 3-day periods prior to mapping. Also indicated in the figure are contours of UKMO PV (dashed lines). The small polar vortex at 850 K left after the late-September sudden warming is seen in late October and

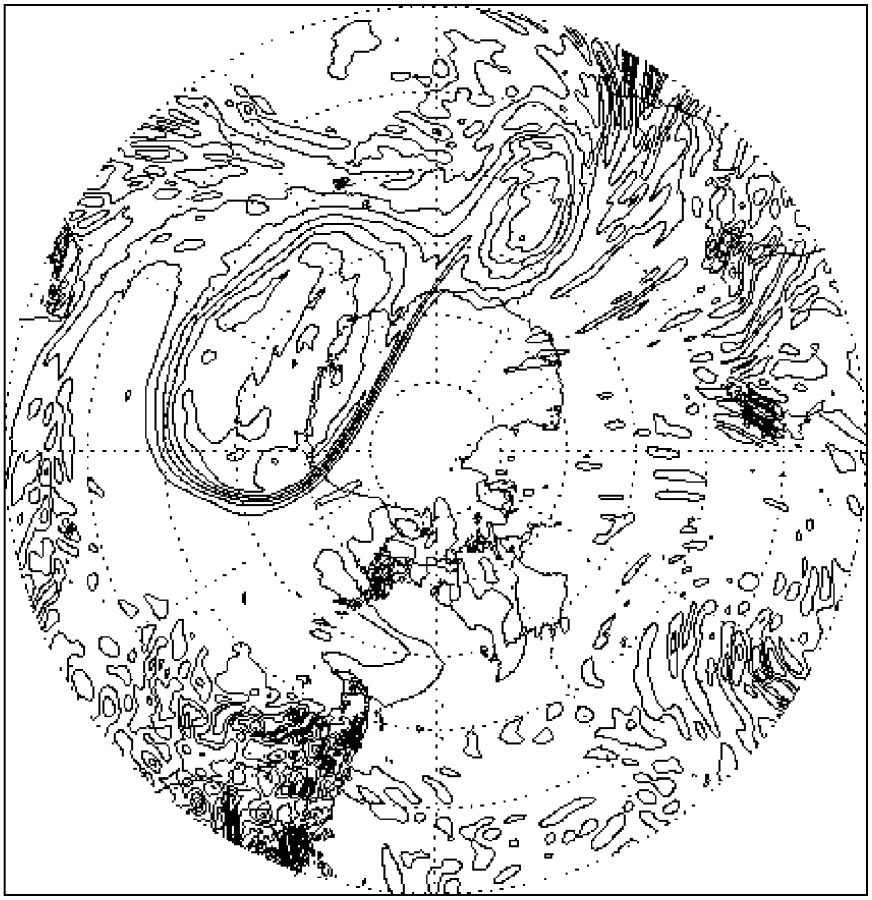

FIG. 5. The PV map as in Fig. 1 at 475 K on 16 Nov 2002.

early November in the moist pool at equivalent latitudes poleward of 70°S and in the tightened PV gradient near 70°S. Equatorward of that latitude, a weak gradient prevails in the midlatitude surf zone. An enhanced gradient delineates the subtropical edge of the surf zone. As time progresses, the characteristic high water vapor mixing ratios are only found at higher and higher equivalent latitudes. The meridional water vapor distribution flattens over mid- and high latitudes by mid-November. At lower potential temperatures, down to 500 K, the meridional PV gradient and the moist pool is maintained until mid-November. The imprint of the longer-lived lower vortex on water vapor is consistent with the PV map in Fig. 5. It also concurs with the studies of Lahoz et al. (1996) and Konopka et al. (2005). The later showed a long-lived and fairly isolated lower-stratospheric vortex in the austral spring of 2002. Below 500 K, the meridional gradient in water vapor flattens and reverses (e.g., at 465 K), a sign of dehydration in the Southern Hemisphere vortex (Nedoluha et al. 2003).

We next analyze maps of MIPAS ozone and water vapor during the vortex breakdown period. Sequences of water vapor and ozone-gridded maps at 850 K from 24 October to 16 November are shown in Figs. 7a and 7b, respectively. We start the description of these events by looking at the water vapor field:

- Over the course of the whole period, the moist vortex is seen to shrink in size and to drift into midlatitudes and eastward toward the Greenwich meridian (0°).
- The pool of moist air left from the vortex disappears from the MIPAS observations altogether by the middle of November.
- The tongue of air pulled out westward during the final breakdown of the vortex, or tongue V, is seen clearly over the period 2–11 November.

A similar picture emerges from the analysis of ozone maps (Fig. 7b): the ozone-poor polar vortex shrinks and moves eastward, but the tongues of polar air are not seen as clearly at this potential temperature level. At the high southern latitudes, ozone decreases rapidly in November, even in a zonal-mean sense (e.g., in Fig. 7b, bottom row). Ozone photochemical destruction catalyzed by the nitrogen cycle is very active in November at this altitude. In ozone-rich parcels advected from midlatitudes to the pole during the final warming, ozone photochemical destruction can be in excess of 100 ppb day^{-1} (Grooss et al. 2005), hence accounting

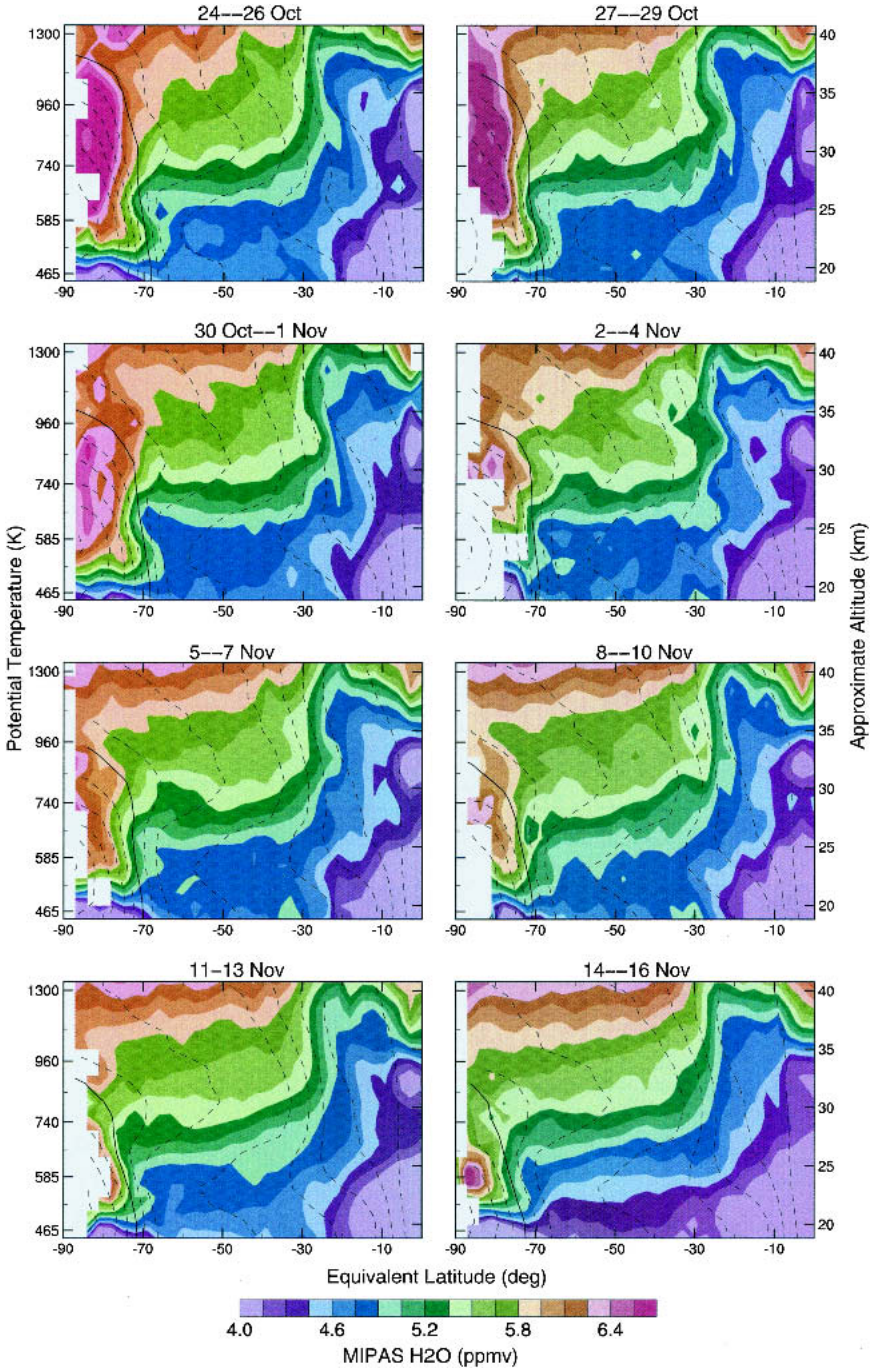

FIG. 6. A sequence of MIPAS water vapor cross sections in equivalent latitude and potential temperature space, from 24 Oct to 17 Nov. Before mapping, data have been combined in 3-day periods. Scaled PV is overlaid (black lines), with the thick line being $-1.6\ 10^{-4}\ s^{-1}$, and the contour interval being $0.2\ 10^{-4}\ s^{-1}$.

for the decrease of the order of 1 ppmv observed by MIPAS over the 10-day period (e.g., 6–16 November).

6. Domain-filling trajectory calculations

Figure 8 shows water vapor maps from a simple transport calculation using a RT model (e.g., Manney et al. 2000, and references therein) for the same days shown in Fig. 7. High-resolution trajectory calculations on an equal area grid with 0.5° equatorial spacing are run back to 24 or 25 October. The tracer fields transported along them are initialized at those times with fields reconstructed from an equivalent latitude/theta-

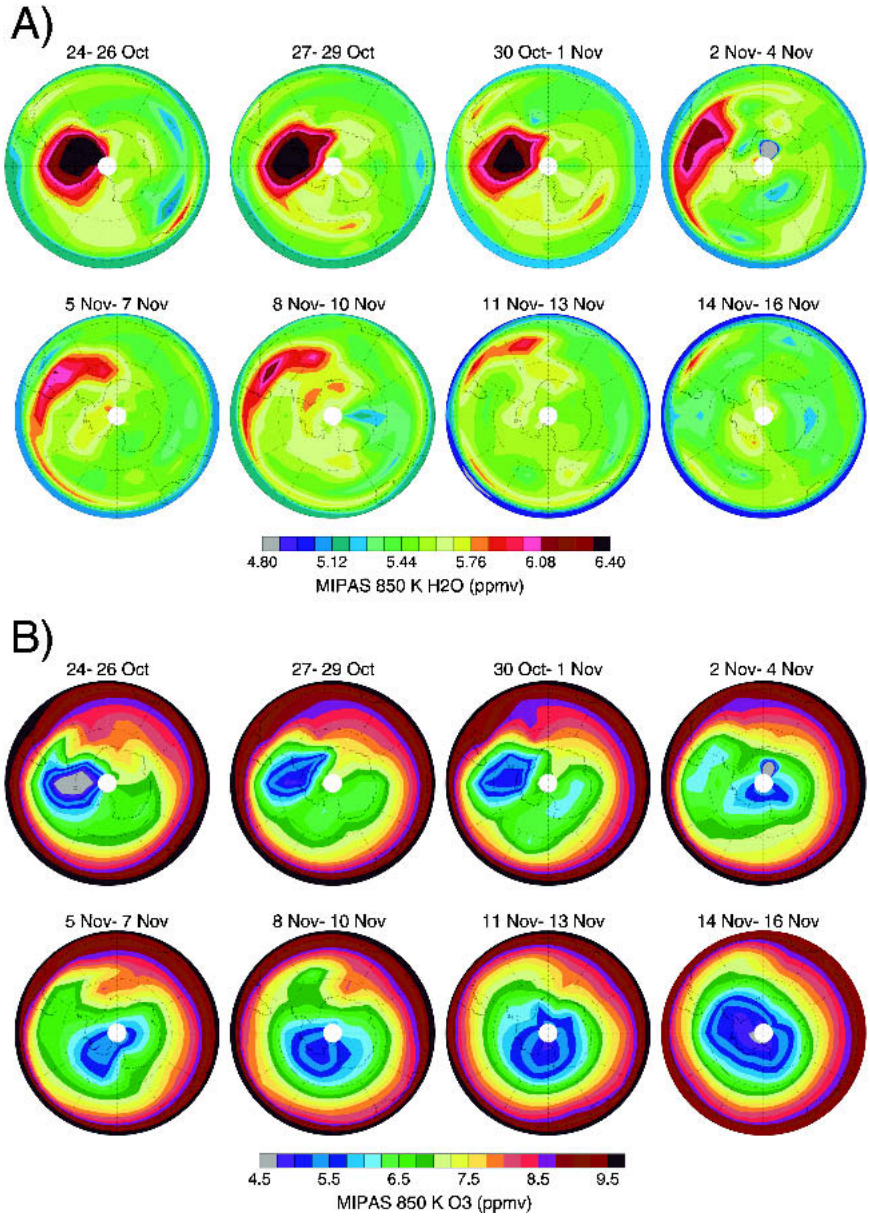

FIG. 7. A sequence of MIPAS (a) water vapor and (b) ozone-gridded maps at 850 K from 24 Oct to 16 Nov. Before binning, data have been combined in 3-day periods. In this orthographic projection and the next two figures, the domain is from −90° to −20°S, and longitudes are same as in Fig. 1.

space pseudoclimatology constructed using the MIPAS water vapor from 24 to 31 October. The further the date is from the day of initialization, the longer the back trajectories, and the more complex the degree of finescale structure in the tracer field. While MIPAS maps are effectively 3-day averages, we keep the central date in fields obtained by the RT method to display finescale features.

The RT maps show clearly the evolution of many of the features seen in coarse-grain fashion in the MIPAS fields. Comparing Fig. 7 with Fig. 8, we see evidence of MIPAS fields capturing the weakened vortex near 90°W during 24–30 October and close correspondence in the shape, position, and size of the decaying vortex through 6 November. On later days, the MIPAS fields still show features corresponding to the large vortex remnants and also to low-latitude air drawn up to 60°S (e.g., near 90°E on 9 November and near 90°E and 90°W on 15 November). The large vortex air tongue V is well into the midlatitudes by 6 November. There is some discrepancy between the RT map and the MIPAS-derived map around 2–4 November, but this is a period when few satellite observations were available (see Table 1).

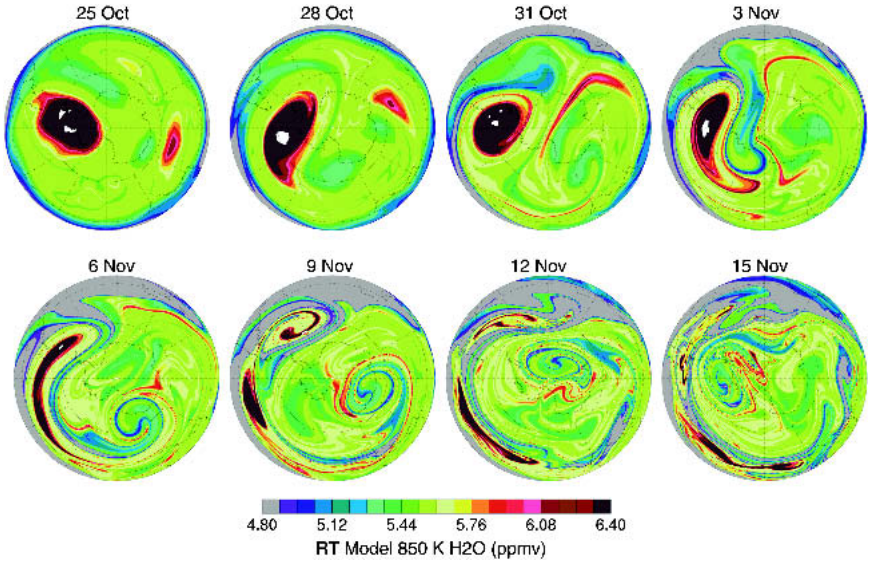

FIG. 8. The RT (see text) maps of water vapor on the 850-K isentropic surface for the date given in each panel. The trajectory calculations are initialized with a 1-week average (24–31 Oct) of MIPAS observations mapped in equivalent latitude.

Hence, we see similar correspondence between the RT maps and the MIPAS observations, in the position and approximate size of the vortex remnants as they decay. Finer-scale features captured in Fig. 8 can be seen in the PV maps (Fig. 1), for example, the coiling of vortex air in the large westward-traveling anticyclone (e.g., around 6–9 November) and the location of the two major, moist remnants of vortex air in the Western Hemisphere (e.g., around 12 November).

7. Comparisons to solar occultation data

In this section, we compare the MIPAS analysis of the vortex breakdown to analyses of ozone and water vapor data from four different satellite-based solar occultation instruments. These instruments are the Halogen Occultation Experiment (HALOE), the Polar Ozone and Aerosol Measurement III (POAM III) instrument, and the Stratospheric Aerosol and Gas Experiments II and III (SAGE II and III). Ozone measurements from POAM III (v3.0), SAGE II (v6.2), and HALOE (v19) have been well validated (e.g., Randall et al. 2003, and references therein). Water vapor measurements from HALOE and POAM III have also been shown to compare well to other measurements. For the time period of most interest here, 24 October to 14 November 2002, the POAM III measurement locations moved approximately linearly in time from 77° to 70°S, while SAGE III measurements moved from about 46° to 43°S. No HALOE measurements were made from 24 October through 5 November, and no SAGE II measurements were made from 24 October through 3 November. From 6–14 November, the HALOE measurement locations moved from about 74° to 64°S, so they were in close proximity to the POAM III measurements. From 4–14 November, the SAGE II measurement locations moved from about 54° to 10°S, thereby filling in the more equatorial latitudes not sampled by the other solar occultation instruments.

Figure 3b compares the 24–30 October MIPAS observations at 850 K to the relationships between equivalent latitude and ozone from the solar occultation instruments for 24–30 October and 7–13 November. The solar occultation curves were derived by fitting the solar occultation data at 850 K with 9-node cubic splines as described by Randall et al. (2004). Note that the solar occultation equivalent latitude is actually the tracer equivalent latitude defined by Allen and Nakamura (2003), interpolated in time and space to the solar occultation measurement locations. Two curves are shown for each time period. This is because photochemical reactions caused the equivalent latitude/ozone relationship to vary as a function of latitude, with ozone increasing toward the equator, even at the same equivalent latitude. Therefore, the equivalent latitude/ozone relationship was defined separately for high-latitude measurements (POAM for 24–30 October; POAM and HALOE for 7–13 November) and midlatitude measurements (SAGE III for 24–30 October; SAGE II and III for 7–13 November). Approximately 85 POAM and SAGE III measurements were used to define each of the ozone solar occultation curves shown in Fig. 3 for the 24–30 October time period; nearly twice that many measurements from POAM, SAGE II and III, and HALOE were used for the curves in the 7–13 November time period. The global MIPAS data are consistent with the 24–30 October solar occultation curves, al-

though there is a hint that the MIPAS data might be slightly higher than the solar occultation data. There is a pronounced decrease in ozone mixing ratios at higher (negative) equivalent latitudes during the 24–30 October time period, indicating that a fairly well contained vortex is present at this altitude.

By 7–13 November during the final warming, the vortex and its remnants at 850 K are located far off the pole. Therefore, the midlatitude SAGE II and III data, rather than POAM and HALOE, define the equivalent latitude/ozone relations at high (negative) equivalent latitudes. The curve for these data (dashed line at higher ozone mixing ratios) has flattened considerably at equivalent latitudes poleward of 60°S, indicative of enhanced mixing between vortex and extravortex air. The 475-K solar occultation ozone data (Figs. 4b–d) do not show evidence of substantial mixing even as late as 20 November. Like MIPAS, the solar occultation ozone data at this altitude retain a pronounced relationship with equivalent latitude, with low ozone sequestered inside the polar vortex.

Figure 3c shows the relationship between equivalent latitude and water vapor from the solar occultation instruments, again superposed on the MIPAS measurements. Here only one solar occultation relationship is shown for each time period, since photochemistry is not a significant factor for water vapor. The water vapor/equivalent latitude curve for 24–30 October was defined by 80 POAM measurements, while the curve for 7–13 November was defined by 120 POAM and HALOE measurements. The character of the water vapor versus equivalent latitude relationship seen in the MIPAS data is similar to that defined by the solar occultation data. Both show an increase in water vapor at high equivalent latitudes, although the solar occultation data show a decrease in water vapor near the center of the vortex. As we show below, the occultation data produce a picture of the vortex breakdown that is qualitatively similar to that derived from the MIPAS data. Because only POAM III and HALOE water vapor measurements are used here, and these instruments only sampled polar (nonvortex) air during the 7–13 November time period, the solar occultation relationship between equivalent latitude and water vapor shown in Fig. 3c is defined only to equivalent latitudes of about 60°S. Thus, whether the water vapor relationship flattens at high equivalent latitudes cannot be determined from these datasets.

Figure 9 is analogous to Fig. 7 in that it shows the 850-K global water vapor distribution derived from the solar occultation measurements. Reconstructed maps have been averaged over 3 days for comparison with Fig. 7. To derive global fields from the sparse solar occultation data, the water vapor mixing ratios were correlated with tracer equivalent latitude, as shown in Fig. 3, and then mapped onto the global grid. Details of the mapping as applied to ozone can be found in Randall et al. (2005). The technique is identical for water vapor, except that here we use POAM III version 4.0 data; since this has not been as well validated as the HALOE data, all measurements are normalized to HALOE (which is approximately 10% lower than POAM at 850 K). Also, the solar occultation water vapor measurements are less certain than ozone and exhibit more variability, so the mapping is not as robust. Thus, we use 21-day increments to define the equivalent latitude/water vapor relationship. Approximately 240 POAM and HALOE measurements de-

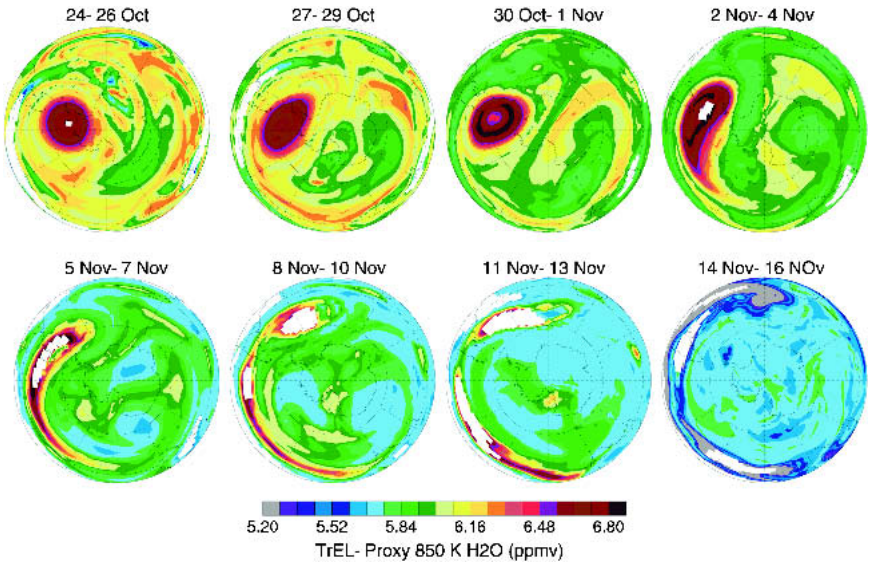

FIG. 9. Global water vapor distributions at 850 K reconstructed from the HALOE and POAM III measurements for a 21-day time period around the central date given in each panel. Maps have then been averaged over the indicated 3-day periods for comparison with MIPAS data.

fined the relationships between equivalent latitude and water vapor that were used to generate the maps in Fig. 9. On the other hand, photochemical considerations are not an issue, so the mapping is latitude independent. Note the different color scale, as the range of water vapor observations is not identical for the MIPAS observations (e.g., Figs. 3 and 7) and the solar occultation data.

The moist vortex air on 24–26 October is centered between longitudes of 60° and 120°W, poleward of 60°S. Figure 9 clearly depicts

- the shrinking vortex, moving equatorward and eastward;
- the tongue V of vortex air that is pulled westward and equatorward from 2 to 10 November;
- the disappearance of the vortex by mid-November;
- and the mostly dry anticyclone progressing westward (e.g., 1–7 November).

8. Discussion

Previous studies of the breakdown of the SH stratospheric vortex have revealed the impact of planetary wave breaking and the vortex interactions upon transport and mixing of minor constituents. Most studies have focused on the initiation and mature stage of the warming. The ultimate fragmentation of the vortex and the dissipation of the major remnants have been little studied before, partly due to a lack of observations with high-resolution and global coverage.

In a case study of the Northern Hemisphere final warming based on infrared satellite observations, a general circulation model and an offline transport model, Hess (1991) showed that large coherent eddies could persist for 2 months after the NH vortex breakdown, trapped and "frozen in" in the westward flow regime. Orsolini (2001) showed, in an offline model simulation with high vertical resolution, that vortex remnants were very resilient and could persist into the summer in the easterlies. They were more rapidly dissipated at altitudes below 20 km, where westerlies prevail and upward extensions of synoptic disturbances were more active. Konopka et al. (2003) used a Lagrangian high-resolution chemical transport model to show that vortex remnants were longer-lived above 20 km and studied the chemistry occurring in the remnants. Piani et al. (2001) also demonstrated that, in the Northern Hemisphere, vortex remnants dispersed more broadly above 20 km than below, where they were bounded by the subtropical jet. Hence, although the final warming is a top-down process, with the vortex breaking first at upper levels, these modeling studies suggest that vortex remnants are in fact long-lived higher up, in the westward flow regime.

We have used 1 month of new ozone and water vapor observations by the MIPAS instrument to reveal the last stages of the life of the SH wintertime stratospheric vortex in 2002 and the first stages of the dissipation of vortex remnants. The satellite observations could coarsely resolve the vortex breakdown and allow tracking of the vortex remnants for a couple of weeks. Further model studies are needed to address the fate of vortex remnants relative to the forming summer easterlies in 2002, over a longer period than the 3–4 weeks that were the focus of the current observational study.

The fact that the shrinking vortex could be followed continuously from one map to the next during the breakdown phase with some consistency between the two tracers owes to the high quality of the MIPAS observations. The degree of correspondence between the MIPAS observations, the reconstructed water vapor from solar occultation data and from high-resolution trajectory calculations, and the analyzed PV and geopotential height is very good (see the dynamical fields and the water vapor field in, e.g., Figs. 1, 7, and 8). The inferences from solar occultation observations and from trajectory-based tracer reconstructions are largely consistent with those from MIPAS measurements.

This study provided an observationally based picture of the main features of the evolution and breakdown of the vortex in spring of 2002. The SH stratospheric zonal circulation reversed earlier than usual at 10 mb, and the summer westward flow is established in the November mean. Coherent and consistent anomalies in ozone and water vapor allow identification of the major remnant from the weakened vortex as it drifted eastward above the southern Atlantic toward the Greenwich meridian and equatorward. A large tongue of air stretched westward out of the vortex and left a significant signature in the MIPAS water vapor and in the reconstructed fields from PV mapping and trajectory transport. The last vortex remnants that can be identified in the satellite observations, especially in water vapor, at that altitude (about 850 K) are found in mid-November over the midlatitudes of the Western Hemisphere. At lower levels (e.g., at 475 K), a small vortex core remained until the end of the period we investigated using MIPAS observations (24 November).

The unusually early Antarctic final warming in 2002 followed a winter that was the most dynamically active, and the only one with a major warming ever observed in the SH. We have shown that the evolution of the vortex and vortex fragments during its breakdown resembles in many ways the behavior seen in previous studies of both the NH and SH winters. Fully understanding the details of how the final warming was influenced by the preceding sudden warming, and whether the final vortex breakdown was triggered primarily by stratospheric vortex interactions or by enhanced tropospheric wave forcing, will require further studies.

Acknowledgments. The lead author was supported by the ESA ENVISAT Calibration and Validation Project, by the Norwegian Space Centre, and by the European Commission through project TOPOZ-III. C. E.

Randall was supported by the Naval Research Laboratory Award N00173-01-01-G007. Work at the Jet Propulsion Laboratory, California Institute of Technology was done under contract with the U.S. National Aeronautics and Space Administration (NASA). The lead author would like to thank S. Migliorini for providing some *ENVISAT* data reading routines.

REFERENCES

Allen, D. R., and N. Nakamura, 2003: Tracer equivalent latitude: A diagnostic tool for isentropic transport studies. *J. Atmos. Sci.,* **60,** 287–304.

——, R. M. Bevilacqua, G. E. Nedoluha, C. E. Randall, and G. L. Manney, 2003: Unusual stratospheric transport and mixing during the 2002 Antarctic winter. *Geophys. Res. Lett.,* **30,** 1599, doi:10.1029/2003GL017117.

Butchart, N., and E. E. Remsberg, 1986: The area of the stratospheric polar vortex as a diagnostic for tracer transport on an isentropic surface. *J. Atmos. Sci.,* **43,** 1319–1339.

Eskes, H., A. Segers, and P. van Velthoven, 2005: Ozone forecasts of the stratospheric polar vortex–splitting event in September 2002. *J. Atmos. Sci.,* **62,** 812–821.

Farrara, J. D., and C. R. Mechoso, 1986: An observational study of the final warming of the southern hemisphere stratosphere. *Geophys. Res. Lett.,* **13,** 1232–1235.

Glatthor, N., and Coauthors, 2005: Mixing processes during the Antarctic vortex split in September–October 2002 as inferred from source gas and ozone distributions from *ENVISAT*–MIPAS. *J. Atmos. Sci.,* **62,** 787–800.

Grooß, J.-U., P. Konopka, and R. Mueller, 2005: Ozone chemistry during the 2002 Antarctic vortex split. *J. Atmos. Sci.,* **62**, 860–870.

Harvey, V. L., R. B. Pierce, T. D. Fairlie, and M. H. Hitchman, 2002: A climatology of stratospheric polar vortices and anticyclones. *J. Geophys. Res.,* **107** (D20), 4442, doi:10.1029/2001JD001471.

Hess, P., 1991: Mixing processes following the final stratospheric warming. *J. Atmos. Sci.,* **48,** 1625–1641.

Hirota, H., K. Kuroi, and M. Shiotani, 1990: Midwinter warmings in the southern hemisphere stratosphere in 1988. *Quart. J. Roy. Meteor. Soc.,* **116,** 919–941.

Hoppel, K. W., R. Bevilacqua, D. Allen, G. Nedoluha, and C. Randall, 2003: POAM III observations of the anomalous 2002 Antarctic ozone hole. *Geophys. Res. Lett.,* **30,** 1394, doi:10.1029/2003GL016899.

Konopka, P., J. U. Grooß, S. Bausch, R. Müller, D. S. McKenna, O. Morgenstern, and Y. Orsolini, 2003: Dynamics and chemistry of vortex remnants in late Arctic spring 1997 and 2000: Simulations with the Chemical Lagrangian Model of the Stratosphere (CLaMS). *Atmos. Chem. Phys. Discuss.,* **3,** 1051–1080.

——, ——, H.-M. Steinhorst, and R. Müller, 2005: Mixing and chemical ozone loss during and after the Antarctic polar vortex major warming in September 2002. *J. Atmos. Sci.,* **62,** 848–859.

Krüger, K., B. Naujokat, and K. Labitzke, 2005: The unusual midwinter warming in the Southern Hemisphere stratosphere 2002: A comparison to Northern Hemisphere phenomena. *J. Atmos. Sci.,* **62,** 603–613.

Lahoz, W. A., and Coauthors, 1996: Vortex dynamics and the evolution of water vapour in the stratosphere of the southern hemisphere. *Quart. J. Roy. Meteor. Soc.,* **122,** 423–450.

Leovy, C. B., C.-R. Sun, M. H. Hitchman, E. E. Remsberg, J. M. Russell III, L. L. Gordley, J. C. Gille, and L. V. Lijak, 1985: Transport of ozone in the middle atmosphere: Evidence for planetary wave breaking. *J. Atmos. Sci.,* **42,** 230–244.

Manney, G. L., J. D. Farrara, and C. R. Mechoso, 1991: The behavior of wave 2 in the Southern Hemisphere stratosphere during late winter and early spring. *J. Atmos. Sci.,* **48,** 976–998.

——, L. Froidevaux, J. W. Waters, L. S. Elson, E. F. Fishbein, R. W. Zurek, R. S. Harwood, and W. A. Lahoz, 1993: The evolution of ozone observed by UARS MLS in the 1992 late winter southern polar vortex. *Geophys. Res. Lett.,* **20,** 1279–1282.

——, R. W. Zurek, M. E. Gelman, A. J. Miller, and R. Nagatani, 1994a: The anomalous Arctic lower stratospheric polar vortex of 1992–1993. *Geophys. Res. Lett.,* **21,** 2405–2408.

——, ——, A. O'Neill, and R. Swinbank, 1994b: On the motion of air through the stratospheric polar vortex. *J. Atmos. Sci.,* **51,** 2973–2994.

——, L. Froidevaux, J. W. Waters, and R. W. Zurek, 1995: Evolution of microwave limb sounder ozone and the polar vortex during winter. *J. Geophys. Res.,* **100,** 2953–2972.

——, Y. J. Orsolini, H. C. Pumphrey, and A. E. Roche, 1998: The 4-day wave and transport of UARS tracers in the austral polar vortex. *J. Atmos. Sci.,* **55,** 3456–3470.

——, H. A. Michelsen, M. L. Santee, M. R. Gunson, F. W. Irion, A. E. Roche, and N. J. Livesey, 1999: Polar vortex dynamics during spring and fall diagnosed using trace gas observations from the Atmospheric Trace Molecule Spectroscopy instrument. *J. Geophys. Res.,* **104,** 18 841–18 866.

——, ——, F. W. Irion, M. R. Gunson, G. C. Toon, and A. E. Roche, 2000: Lamination and polar vortex development in fall from ATMOS long-lived trace gases observed during November 1994. *J. Geophys. Res.,* **105,** 29 023–29 038.

Mechoso, C. R., A. O'Neill, V. D. Pope, and J. D. Farrara, 1988: A study of stratospheric warming of 1982 in the southern hemisphere. *Quart. J. Roy. Meteor. Soc.,* **114,** 1365–1384.

Nedoluha, G. E., R. M. Bevilacqua, and K. W. Hoppel, 2002: POAM III measurements of dehydration in the Antarctic and comparisons with the Arctic. *J. Geophys. Res.,* **107,** 8290, doi:10.1029/2001JD001184.

Newman, P. A., and E. R. Nash, 2005: The unusual Southern Hemisphere stratosphere winter of 2002. *J. Atmos. Sci.,* **62,** 614–628.

Orsolini, Y. J., 2001: Long-lived tracer patterns in the summer polar stratosphere. *Geophys. Res. Lett.,* **28,** 3855–3858.

Piani, C., W. A. Norton, A. M. Iwi, E. A. Ray, and J. W. Elkins, 2001: Transport of ozone-depleted air on the breakup of the stratospheric polar vortex in spring/summer 2000. *J. Geophys. Res.,* **107,** 8270, doi:10.1029/2001JD000488.

Randall, C. E., and Coauthors, 2003: Validation of POAM III ozone: Comparisons with ozonesonde and satellite data. *J. Geophys. Res.,* **108,** 4367, doi:10.1029/2002JD002944.

——, G. L. Manney, D. R. Allen, R. M. Bevilacqua, C. Trepte, W. Lahoz, and A. O'Neill, 2005: Reconstruction and simulation of stratospheric ozone distributions during the 2002 austral winter. *J. Atmos. Sci.,* **62,** 748–764.

Simmons, A., and Coauthors, 2005: ECMWF analyses and forecasts of stratospheric winter polar vortex breakup: September 2002 in the Southern Hemisphere and related events. *J. Atmos. Sci.,* **62,** 668–689.

Swinbank, R., and A. O'Neill, 1994: A stratosphere–troposphere data assimilation system. *Mon. Wea. Rev.,* **122,** 686–702.

Waugh, D. W., and W. J. Randel, 1999: Climatology of Arctic and Antarctic polar vortices using elliptical diagnostics. *J. Atmos. Sci.,* **56,** 1594–1613.

——, ——, S. Pawson, P. A. Newman, and E. R. Nash, 1999: Persistence of the lower stratospheric polar vortices. *J. Geophys. Res.,* **104,** 27 191–27 201.

Yamazaki, K., and C. R. Mechoso, 1985: Observation of the final warming in the stratosphere of the Southern Hemisphere during 1979. *J. Atmos. Sci.,* **42,** 1198–1205.